CHAPTER III

RESULTS

3.1 Isolation and characterization of *A. halophytica* Na^+/H^+ antiporter, *apnha*P

3. 1. 1 Isolation of *A. halophytica* Na^+/H^+ Antiporter

By using the mixed oligonucleotides of two highly conserved regions among several NhaP-type antiporters, DNA fragments of *apnha*P gene of an expected size (approximately 0.3 kbp) were obtained using PCR condition as follows: cycle 1 (1X) initial denaturation at 96°C for 12 min, cycle 2 amplification (50X) by denaturing at 96°C for 30 sec; annealing at 50°C for 30 sec and elogation at 72°C for 30 sec, cycle 3 (1X) final extension at 72°C for 7 min. A DNA fragment was sequenced and blasted with database in Genbank. It showed high homology to NhaP type antiporter. Then, the upstream and downstream regions of the fragment were amplified by the inverse PCR method. The nucleotide sequence of the entire 2431 bp was determined (Fig. 3.1 A). The sequence analysis revealed one possible open reading frame, *apnha*P, spanning positions 796 to 2361. The predicted gene product consists of 521 amino acids with a molecular mass of 56,881 Da (ApNhaP). The upstream sequence of the first Met revealed the presence of -10 (ATGAAT) and -35 (TACACT) consensus sequences (Fig. 3.1B). At further upstream region spanning positions 185 to 676, another open reading frame encoding a low-potential *c*-cytochrome associated with the photosystem II (Cyt. *c*550), was found. The homology search revealed that ApNhaP is highly homologous to the Na^+/H^+ antiporters from eucaryotes (SOS1, NHEs, AtNHX1, and NHX1) and procaryotes (NhaP, SynNhaP, and SynNhaP2) as shown in Fig. 3.2. Here, SynNhaP2 is the second NhaP-type

antiporter found in *Synechocystis* sp. PCC 6803 (Hamada et al., 2001). ApNhaP showed the highest homology to SynNhaP (*c.* 61% identity in amino acids). The conserved amino acid residues among this group are highlighted in black and the conservative substitutions are shown by dot (Fig. 3.2A). Analysis of the hydropathy plot (Kyte and Doolittle, 1982) and the TM prediction program (Hofman and Stoffel, 1992) predicted 11 putative TM segments in ApNhaP (Fig. 3.3). The Asp139 in ApNhaP was the conserved ionic amino acid in membrane spanning region whose importance for the exchange activity has been shown by the mutagenesis analysis of SynNhaP (Hamada et al.. 2001). The ApNhaP contained a long hydrophilic C-terminal tail as shown in the case of eucaryotic Na^+/H^+ antiporters, but not in the case of NhaP from *P. aeruginosa*. These data indicate that a halotolerant cyanobacterium *A. halophytica* contains an Na^+/H^- antiporter homologous to eucaryotic ones.

A)

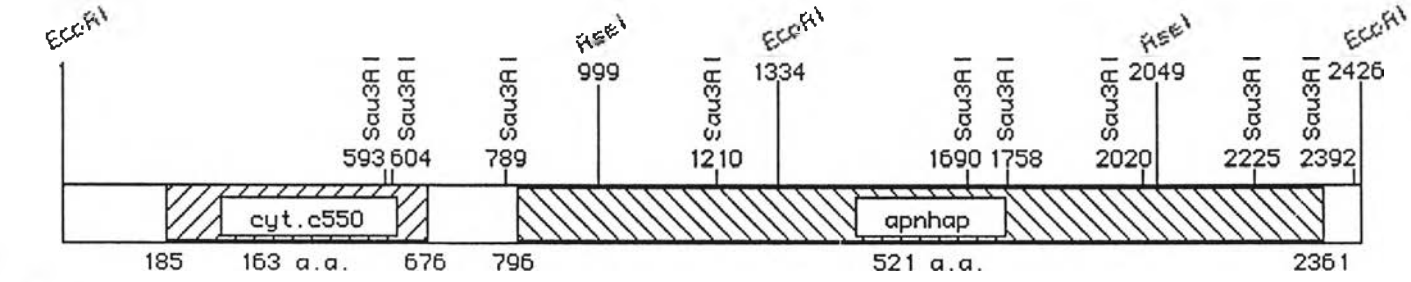

B)

```
617 ATT CTC AGT CAA CCG AAA AGT CCG AGG AAG CAA TGG GGT GAC GGT AAA GTC TAT AAC TAA
     I   L   S   Q   P   K   S   P   R   K   Q   W   G   D   G   K   V   Y   N   *
677 GGC TTA ACT GAT GAC CTC AAA GTC TGT CTC GTG TCC CTC CTC ATG AAT TTG GGG AGG GAT
                                                          -35
737 TTT TAG TAC ACT TAT TAC AAA TAA ACG TCA CGA TTA AAG TTA CAG GAA AGC CTG ATC CCT
          -10
796 ATG ACT ATT GAA GCA GCA ATG GGA GAA GAA GCC ATT AAG GAA AAT TTA GAA CAG TTC CTG
     M   T   I   E   A   A   M   G   E   E   A   I   K   E   N   L   E   Q   F   L
```

Figure 3.1 A) Genomic organization of the *apnha*P locus of *A. halophytica.*

B) Nucleotide sequence of the junction region between *apnha*P and *cyt. c550.*

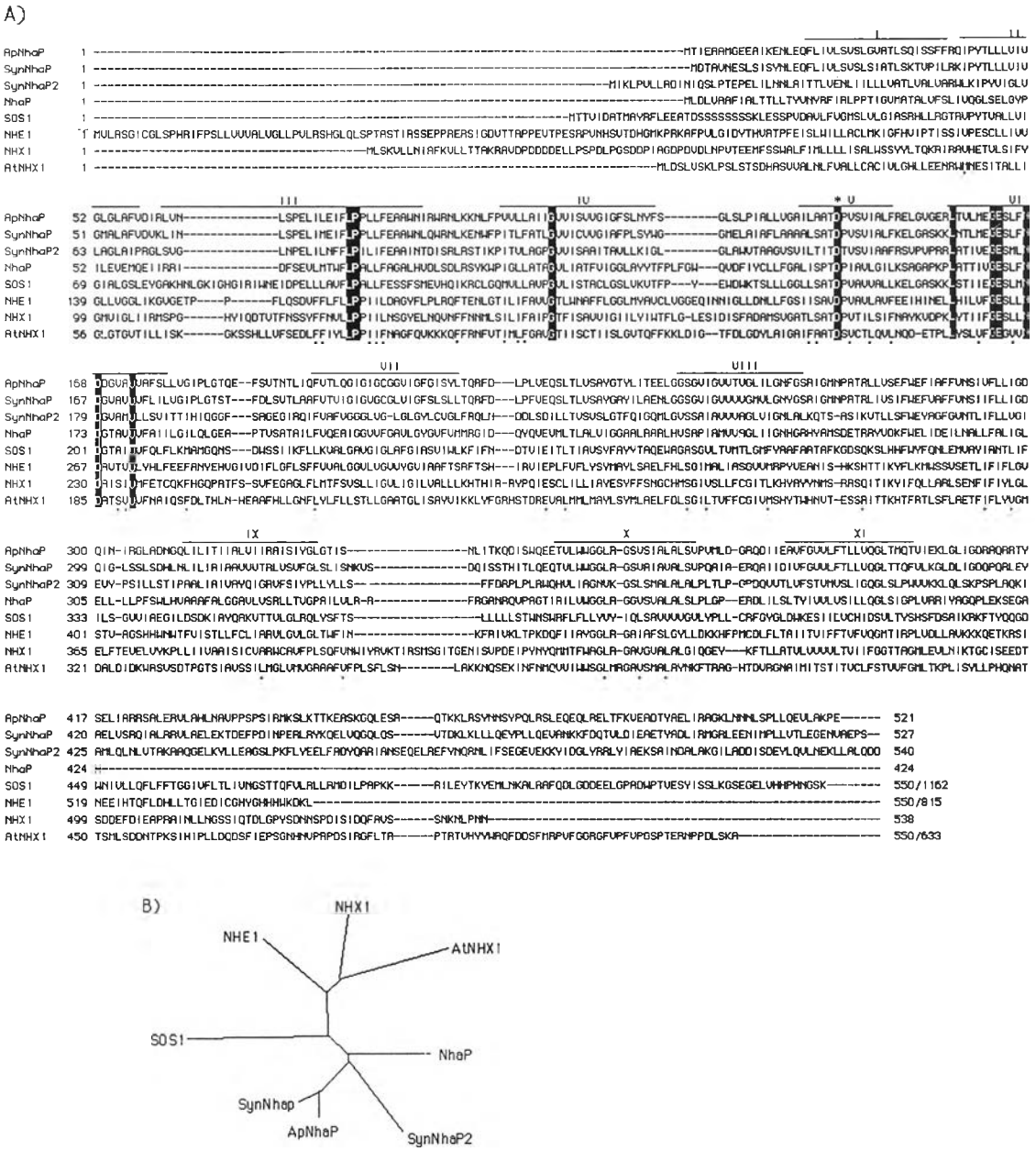

Figure 3.2 A) Alignment of the deduced amino acid sequences of Na^+/H^+ antiporters from eight organisms. B) Phylogenetic analysis of eight Na^+/H^+ antiporters.

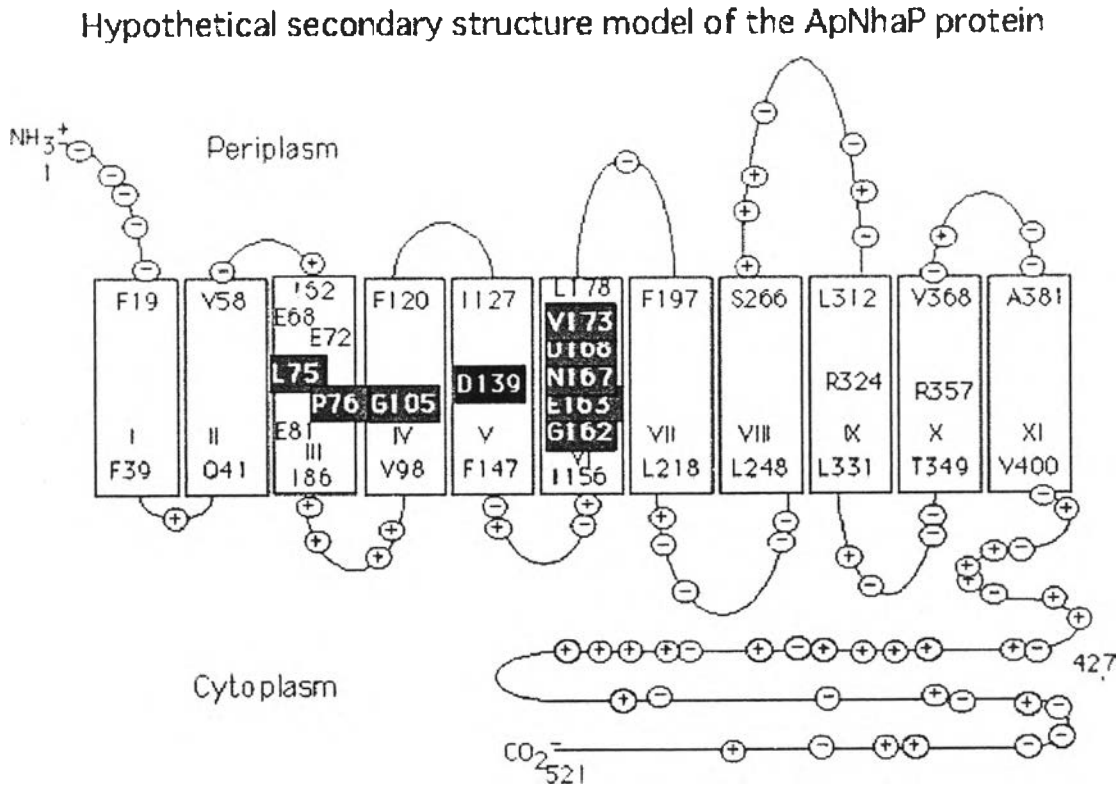

Figure 3.3 Topology model of ApNhaP

3. 1. 2 Construction of expression plasmids (pANhaP and pSNhaP) and complemetation test with the salt-sensitive mutant *E.coli* TO114

The full length Na^+/H^+ antiporter *gene, apnha*P, was amplified by ANP-NcoI and APN-HindIII as the primers and performed in the PCR condition as follows: cycle 1 (1X) initial denaturation at 96°C for 12 min, cycle 2 amplification (50X) by denaturing at 96°C for 30 sec; annealing at 50°C for 30 sec and elongation at 72°C for 3 min, cycle 3 (1X) final extension at 72°C for 7 min. The PCR product was analyzed by 1 % agarose gel electrophoresis. A single band at approximately 1.6 kb was observed as shown in Fig. 3.4. PCR fragment was double digested with *Nco*I and *Hind*III and ligated into *Nco*I/*Hind*III sites of the digested pTrcHis2C expression vector. After transfer to *E.coli* DH5α, the plasmid was extracted from the transformant. The insert fragment approximately 1.6 kb was checked by double digestion with *Nco*I/*Hind*III (Fig 3.5). The clone harboring pANhaP was picked up and grown from which plasmid was extracted and transferred to *E.coli* TO114.

The expressing cells, pANhaP and pSNhaP were tested for complementation with the salt-sensitive *E.coli* mutant TO114. Fig 3.6A shows the growth rate of expressing cells and control (vector alone) in LBK medium at pH 7.0 and 37°C. *E. coli* TO114 cells transformed with pANhaP could grow with a similar rate to that of the TO114 cells transformed with pSNhaP and pTrcHis2C in LBK medium at pH 7.0 and 37°C. However, due to the absence of Na^+/H^+ antiporter genes (*nhaA*, *nhaB*, and *chaA*) in TO114, the E.coli cells transformed with pTrcHis2C could not grow in the presence of 0.2 M NaCl (Fig. 3.6B). In contrast, the *E. coli* cells transformed with pANhaP or pSNhaP could grow (Fig. 3.6B). Interestingly, the TO114 cells transformed with pANhaP grow slightly faster than those transformed with pSNhaP (Fig. 3.6B).

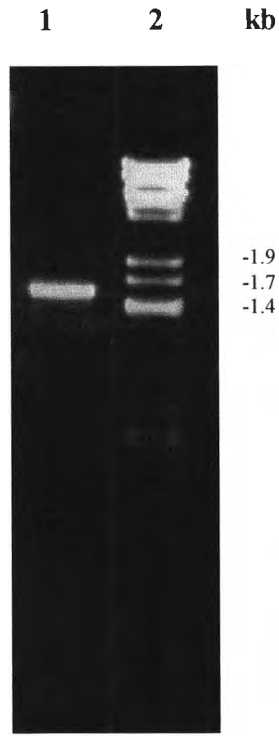

Figure 3.4 PCR product of *apnha*P analysed on 1 % agarose electrophoresis

Lane 1 : PCR product corresponding to 1.6 kb

Lane 2 : λ DNA/*Eco*RV

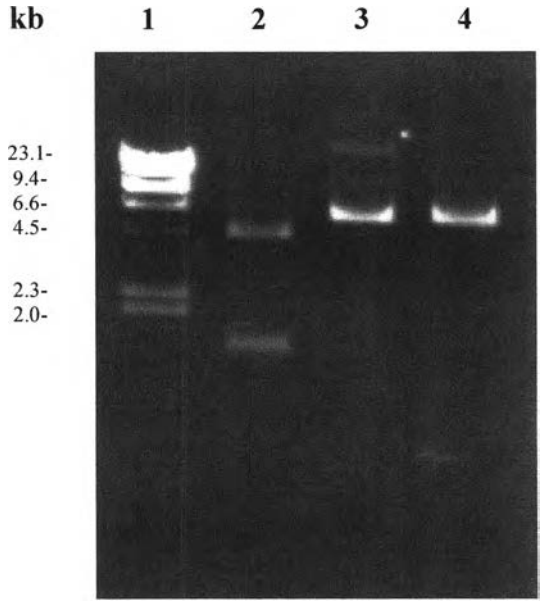

Figure 3.5 Analysis of pANhaP digested with *Nco*I and *Hind*III on 1% agarose gel electrophoresis

Lane 1 : λ/*Hind*III

Lane 2 : pANhaP double digestion with *Nco*I and *Hind*III

Lane 3 : pANhaP digestion with *Nco*I

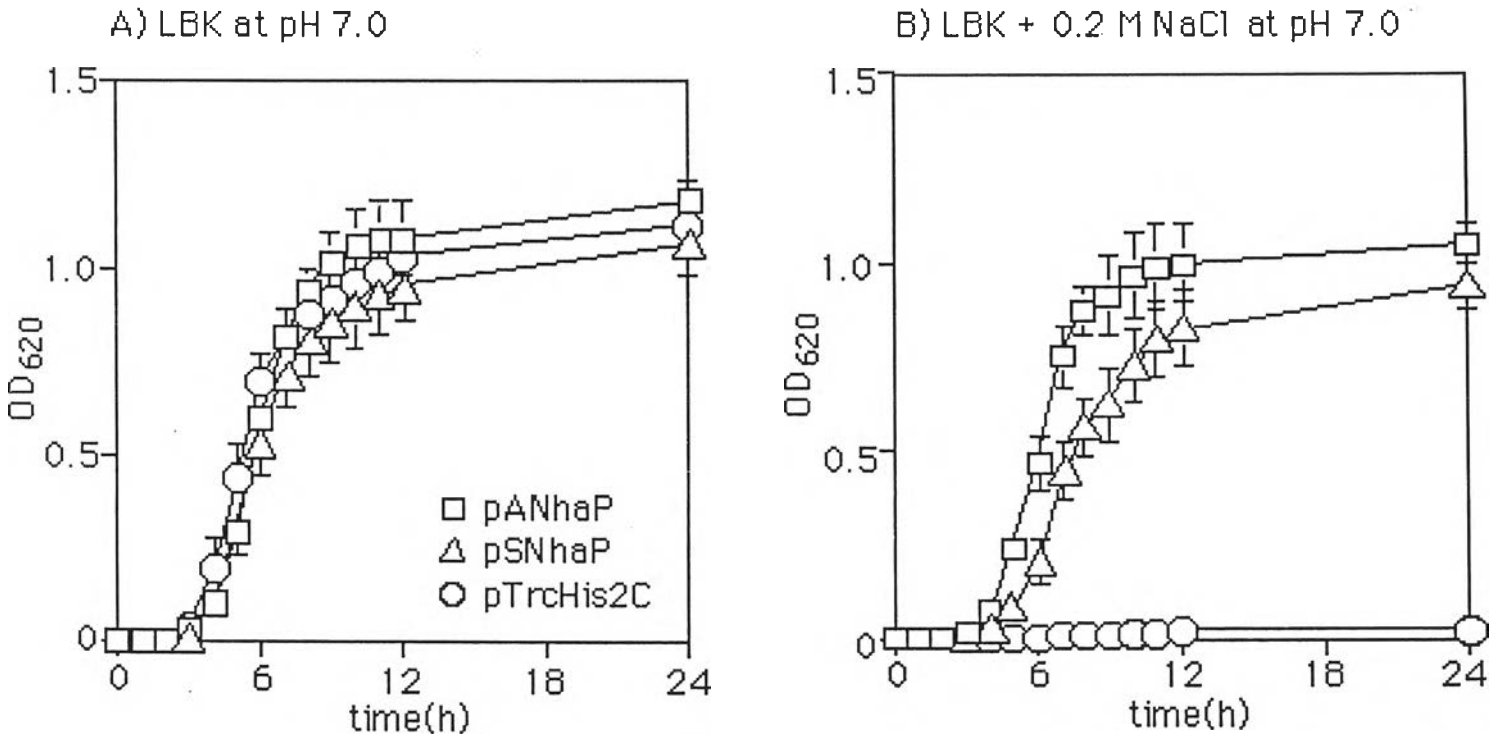

Figure 3.6 Effects of NaCl on the growth rates of three kinds of *E. coli* cells. The control and transformant cells at logarithmic phase in LBK medium were transferred to the fresh LBK medium containing indicated concentrations of NaCl at pH 7.0. A) Time courses of growth in LBK medium. B) Time courses of growth in LBK containing 0.2 M NaCl. Control cells, circle; ApNhaP-expressing cells, square; SynNhaP-expressing cells, triangle. Each value shows the average of three independent measurements .

Figure 3.6B suggests the different complementation ability between ApNhaP and SynNhaP. It was of interest, therefore, to examine other conditions which cause more clear differences in the complementation ability in these two antiporters. Figure 3.7A-C shows that at the growth temperature 30°C, the TO114 cells transformed with pANhaP could grow slightly faster than those transformed with pSNhaP at alkaline pH in LBK medium. Under these conditions, ApNhaP could complement the salt-sensitive phenotype of TO114 cells when the growth medium contained 0.2 M NaCl whereas SynNhaP could not (Fig. 3.7B). TO114 cells transformed with pANhaP could grow even in the presence of 0.5 M NaCl (Fig. 3.7C). These differences in complementation ability were not observed at lower pHs. The above results indicate that ApNhaP could complement more efficiently than SynNhaP at alkaline pH.

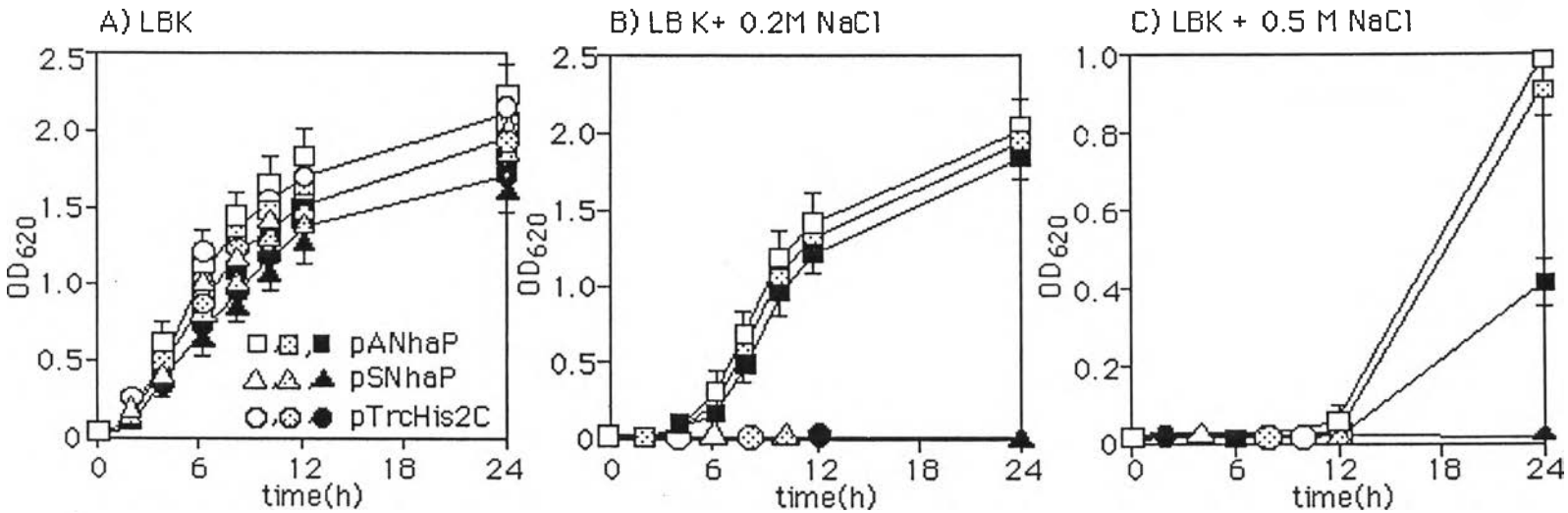

Figure 3.7 LBK medium were transferred to the fresh LBK medium containing indicated concentrations of NaCl and pH. The growth temperature was 30°C. Time courses of growth in LBK medium containing A) 0 M NaCl, B) 0.2 M NaCl, and C) 0.5 M NaCl. ApNhaP-expressing cells at pH 8.0, open square; pH 8.5, hatched square; pH 9.0, closed square. SynNhaP-expressing cells at pH 8.0, open triangle; pH 8.5, hatched triangle; pH 9.0, closed triangle. Control cells at pH 8.0, open circle; pH 8.5, hatched circle; pH 9.0, closed circle. Each value shows the average of three independent measurements

3. 1. 3 Na^+/H^+antiporter activity

To examine directly the antiporter activity of ApNhaP, the everted membrane vesicles were prepared and their antiporter activities were monitored by measuring the lactate induced fluorescence quenching (Q) and salt induced fluorescence dequenching (ΔQ). As shown in an upper panel of Fig. 3.8, the dequcnching (ΔQ x100/Q) was observed upon the addition of NaCl in the ApNhaP-expressing cells, but not in the control (pTrcHis2C) cells, indicating that ApNhaP has Na^+/H^+ antiporter activity. Figure 3.8A shows that the dequenching of fluorescence by ApNhaP was observed over a wide range of pH between 5 and 9 which is similar to that by SynNhaP (Hamada et al., 2001), but quite different from that by *E. coli* NhaA. In *E. coli* NhaA, the antiporter activity could not be observed below pH 7.5 while the activity increased with increasing pH (Padan and Schuldiner, 1996).

To examine the ion specificity of ApNhaP, the dequenching was measured upon the addition of different cations. In contrast to most Na^+/H^+ antiporters which could catalyze the exchange between Li^+ and H^+, ApNhaP showed virtually no activity of Li^+/H^+ antiporter at various pHs (Fig. 3.8B). Moreover, it was found that ApNhaP could exhibit Ca^{2+} antiporter activity at neutral or alkaline pH (Fig. 3.8C) whereas only small or no antiporter activity was observed for K^+/H^+ or Mg^{2+}/H^+, respectively (Fig 3.9). These results indicate that ApNhaP is an antiporter with novel ion specificity.

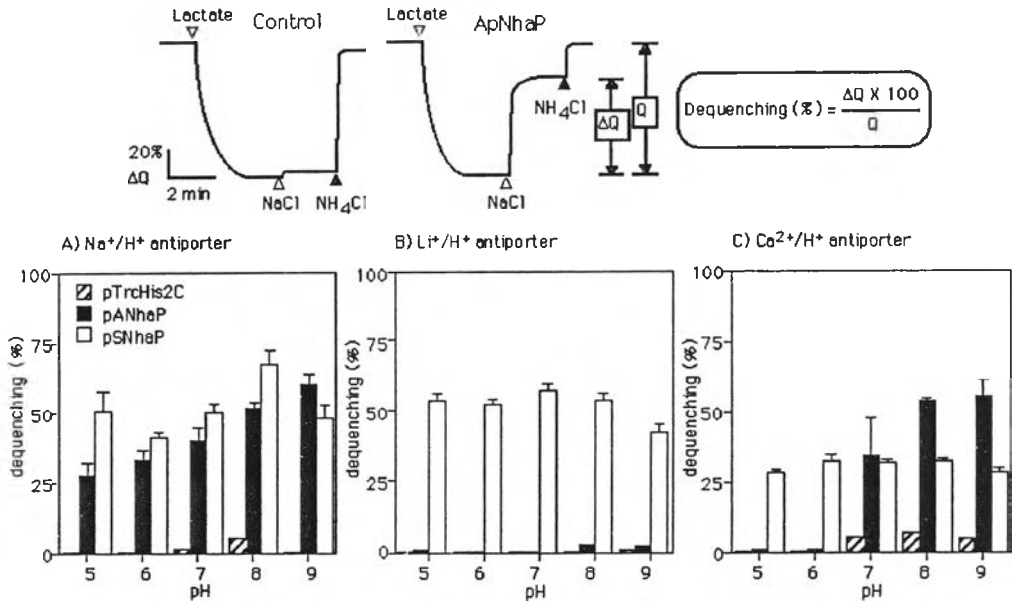

Figure 3.8 The activities of Na^+/H^+ antiporters measured by the acridine orange fluorescence quenching method. The control *E. coli* cells and *E. coli* cells expressing ApNhaP and SynNhaP were grown in LBK medium without addition of extra salts. From these cells the everted membrane vesicles were prepared. The antiporter activity was measured as described in Materials and Methods. The upper panel shows typical quenching patterns in the ApNhaP-expressing and control (pTrcHis2C) cells. Panels A), B), and C) show the pH depemdence of Na^+/H^+-, Li^+/H^+- and Ca^{2+}/H^+-antiporter activities, respectively. The final concentrations of salts (NaCl, LiCl, and $CaCl_2$) were 5 mM Each value shows the average of three independent measurements.

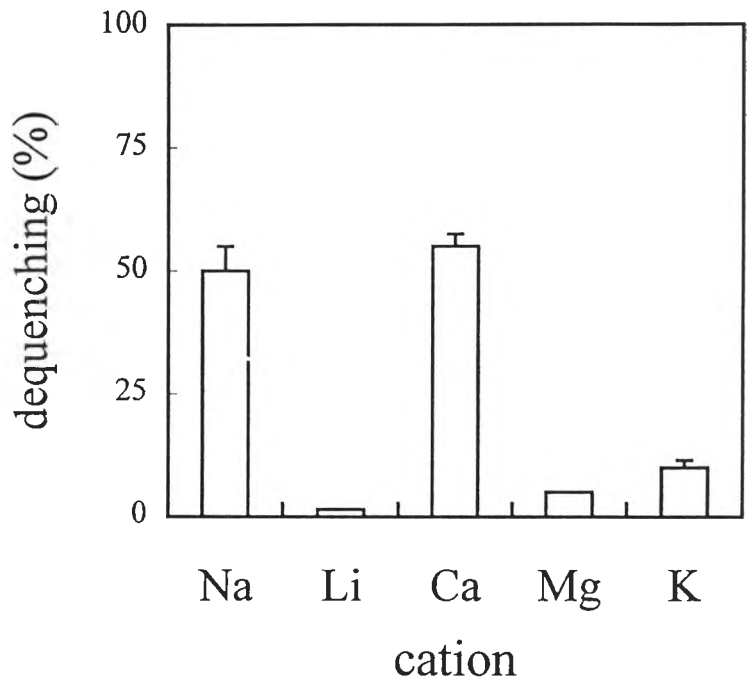

Figure 3.9 The activities of Cation/Proton antiporters measured by the acridine orange fluorescence quenching method. The *E. coli* cells expressing ApNhaP were grown in LBK medium without addition of extra salts. From these cells the everted membrane vesicles were prepared. The antiporter activity was measured as described in Materials and Methods.

Since the above results indicate that ApNhaP has an exchange activity between Ca^{2+} and H^+, but not between Li^+ and H^+, it was of interest to examine whether these ion specificities could be demonstrated in the complementation of salt-sensitive phenotypes of *E. coli* mutant cells. As shown in Fig. 3.10A, the TO114 cells expressing ApNhaP could not grow in LBK medium containing 4 mM LiCl at pH 8.0 whereas the TO114 cells expressing SynNhaP could grow. In contrast, Fig. 3.10B indicates that the TO114 cells expressing ApNhaP could grow well in the TrisE medium containing 0.1 M $CaCl_2$ at pH 8.0 (Brockman and Heppel, 1968.), but the TO114 cells expressing SynNhaP grew slowly. In both cases, the control cells (vector only) could not grow (Figs. 3.10A and 3.10B). These results are consistent with the results of Li^+/H^+ and Ca^{2+}/H^+ antiporter activities of ApNhaP and SynNhaP (Figs. 3.8B and 3.8C) although the growth rate of SynNhaP expressing cells in Ca^{2+} containing medium appeared to be slower than that anticipated from the Ca^{2+}/H^+ exchange activity of SynNhaP (Figs 3.10B vs 3.8C).

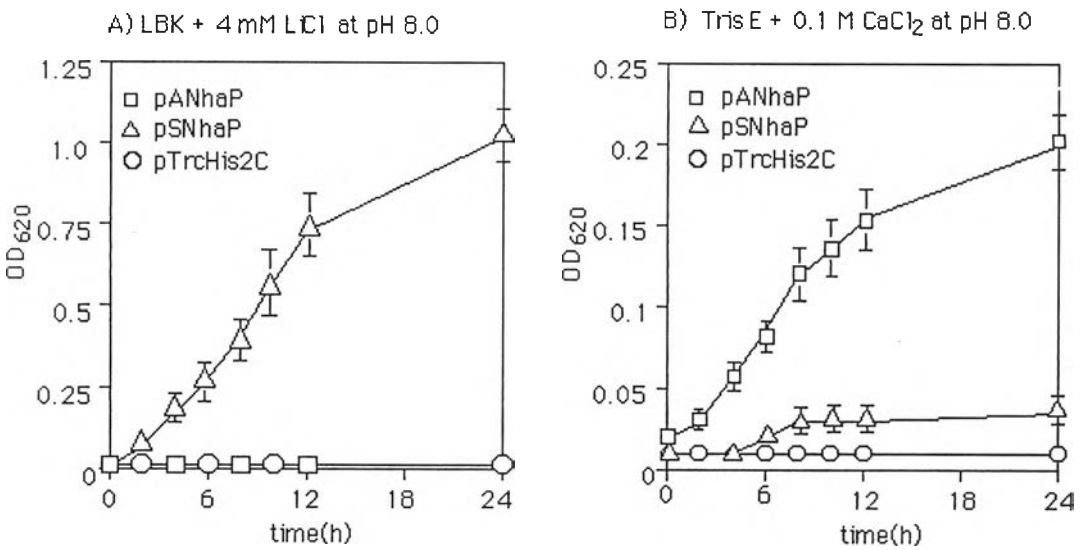

Figure 3.10 Effects of LiCl and $CaCl_2$ on the growth rates of three kinds of *E. coli* cells. The control and transformant cells at logarithmic phase in LBK medium were transferred to the LBK or TrisE medium containing indicated concentrations of LiCl or $CaCl_2$, respectively. Other experimental conditions were the same as those in Fig. 3.6. Each value shows the average of three independent

3. 1. 4 Construction of chimeric gene between *apnha*P (Na^+/H^+ antiporter gene from *Aphanothece halophytica*) and *synnha*P (Na^+/H^+ antiporter gene from *Synechocystis* sp. PCC6803)

Chimeric genes, *apsynnha*P and *synapnha*P which exchanged C-terminal part with each other were constructed. Fig. 3.11 shows the schematic secondary structure model of chimeric Na^+/H^+ antiporters. The number of positive and negative charges on the C-terminal hydrophilic tails are indicated. Construction of the anticipated chimeric genes were confirmed by restriction enzyme digestion (Fig. 3.12 and 3.13) and DNA sequencing.

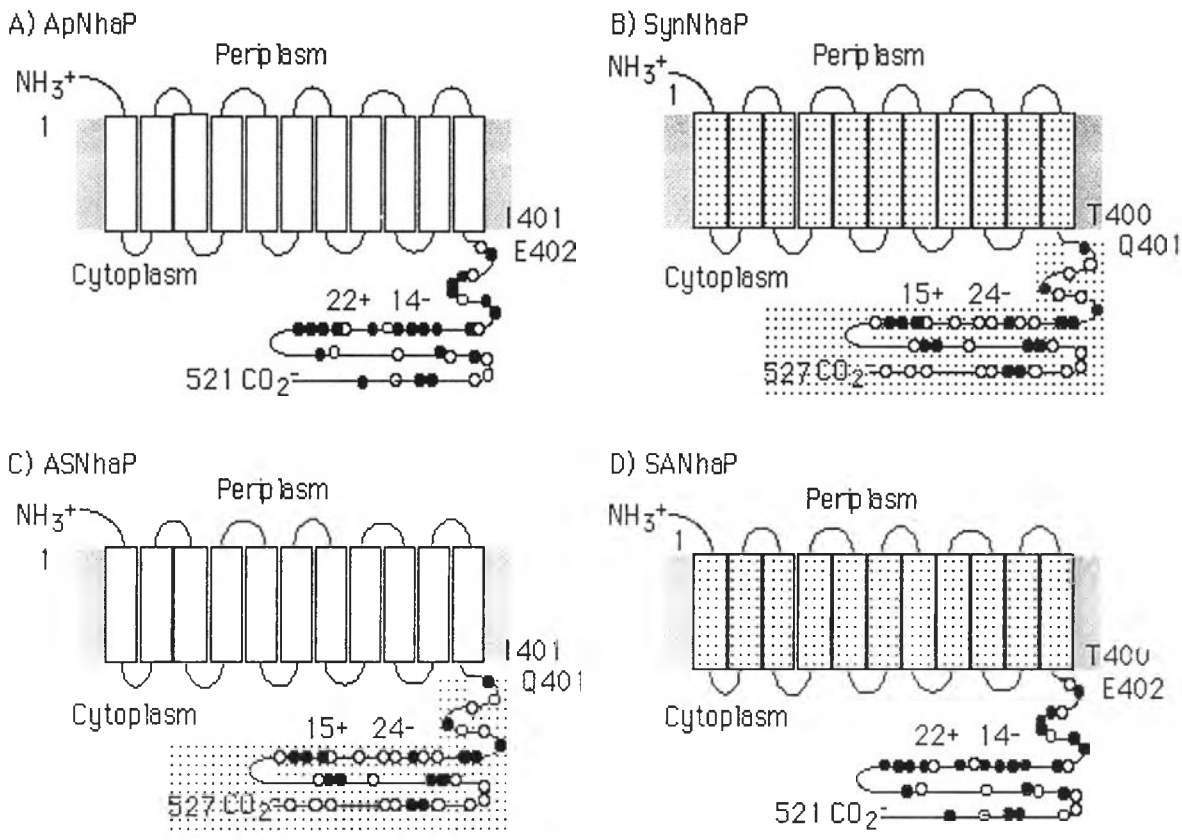

Figure 3.11 Schematic figure for construction of chimeric genes pASNhaP and pSANhaP

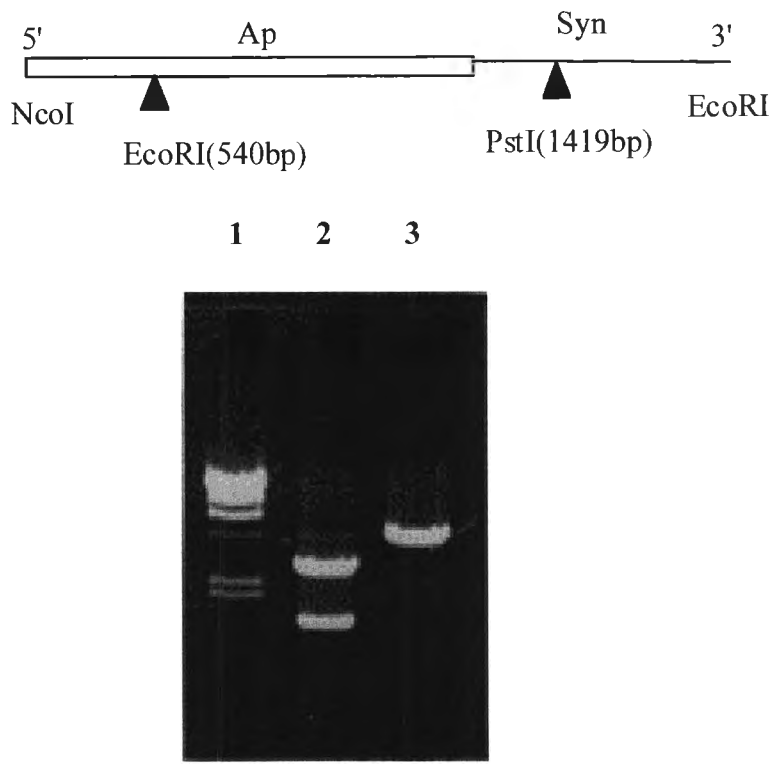

Figure 3.12 Analysis of pASNhaP digested with restriction enzymes on 1% agarose gel electrophoresis

Lane 1 : λ DNA /*Hind*III

Lane 2 : pASNhaP double digestion with *Nco*I and *Pst*I

Lane 3 : pASNhaP digestion with *Nco*I

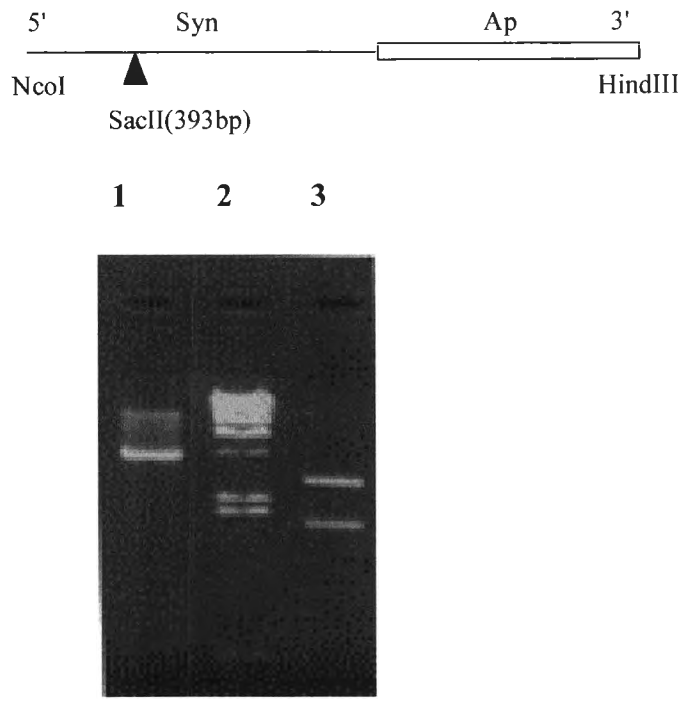

Figure 3.13 Analysis of pSANhaP digested with restriction enzymes on 1% agarose gel electrophoresis

Lane 1 : pSANhaP double digestion with *EcoR*I

Lane 2 : λ DNA/HindIII

Lane 3 : pSANhaP digestion with *Nco*I/*Hind*III

Previously, it was shown that the partial deletion of C-terminal tail decreased the Na^+/H^+ antiporter activity of SynNhaP (Hamada et al., 2001). Although ApNhaP showed the highest homology to SynNhaP, the charges on the C-terminal tail of these two antiporters are significantly different, 22 basic and 14 acidic amino acids in ApNhaP and 15 basic and 24 acidic amino acids in SynNhaP. Therefore, the chimeric antiporters, ASNhaP and SANhaP, in which the long C-terminal tails of ApNhaP and SynNhaP were replaced with those of SynNhaP and ApNhaP, respectively, were constructed as shown in Fig. 3.11. The exchange activities of chimeras were measured using the everted membrane vesicles. Figure 3.14 shows that the ASNhaP chimera exhibited comparable Na^+/H^+, Li^+/H^+, and Ca^{2+}/H^+ exchange activities to those of the parental ApNhaP (Figs.3.8). Interestingly, the Li^+/H^+ exchange activity which was virtually non-detectable in ApNhaP (Fig. 3.8B) could be clearly observed in the ASNhaP chimera (Fig.3.14B). On the other hand, the SANhaP chimera showed reduced exchange activities of both Na^+/H^+ and Li^+/H^+ as compared to the parental SynNhaP (Fig. 3.14 vs. Fig. 3.8). Furthermore, the Ca^{2+}/H^+ exchange activity in the SANhaP chimera appeared to be pH-dependent, i.e. increased activity was observed at neutral or alkaline pH (Fig. 3.14C), which was in contrast to that observed for the parental SynNhaP, showing relatively unchanged activity irrespective of the pH (Fig. 3.8C). These results suggest that the C-terminal region plays a role for the ion specificity of ApNhaP and SynNhaP although some activity data do not reconcile with this viewpoint. For example, the SANhaP chimera had low Na^+/H^+ exchange activity compared with that of ApNhaP and SynNhaP (Figs. 3.14A and 3.8A) and the Ca^{2+}/H^+ exchange activity of ASNhaP chimera was pH-dependent which is the same as that for the parental ApNhaP, but different from that for the

SynNhaP (Fig. 3.8C). These results suggest that the ion specificities of ApNhaP and SynNhaP are also affected by the structures in TM regions as assumed in most cases of Na^+/H^+ antiporters (Padan and Schuldiner, 1996).

The exchange activity data of chimeras were further substantiated by the complementation analysis. As shown in Fig. 3.15, the ASNhaP chimera could complement the Na^+-, Li^+-, and Ca^{2+}-sensitive phenotypes of *E. coli* mutant whereas the SANhaP chimera could hardly complement the Na^+- and Li^+-sensitive phenotype of *E. coli* mutant. The growth rate of *E. coli* mutant cells expressing SANhaP was slower than that anticipated from the Ca^{2+}/H^+ exchange activity of SANhaP chimera (Figs. 3.15C and 3.14C).

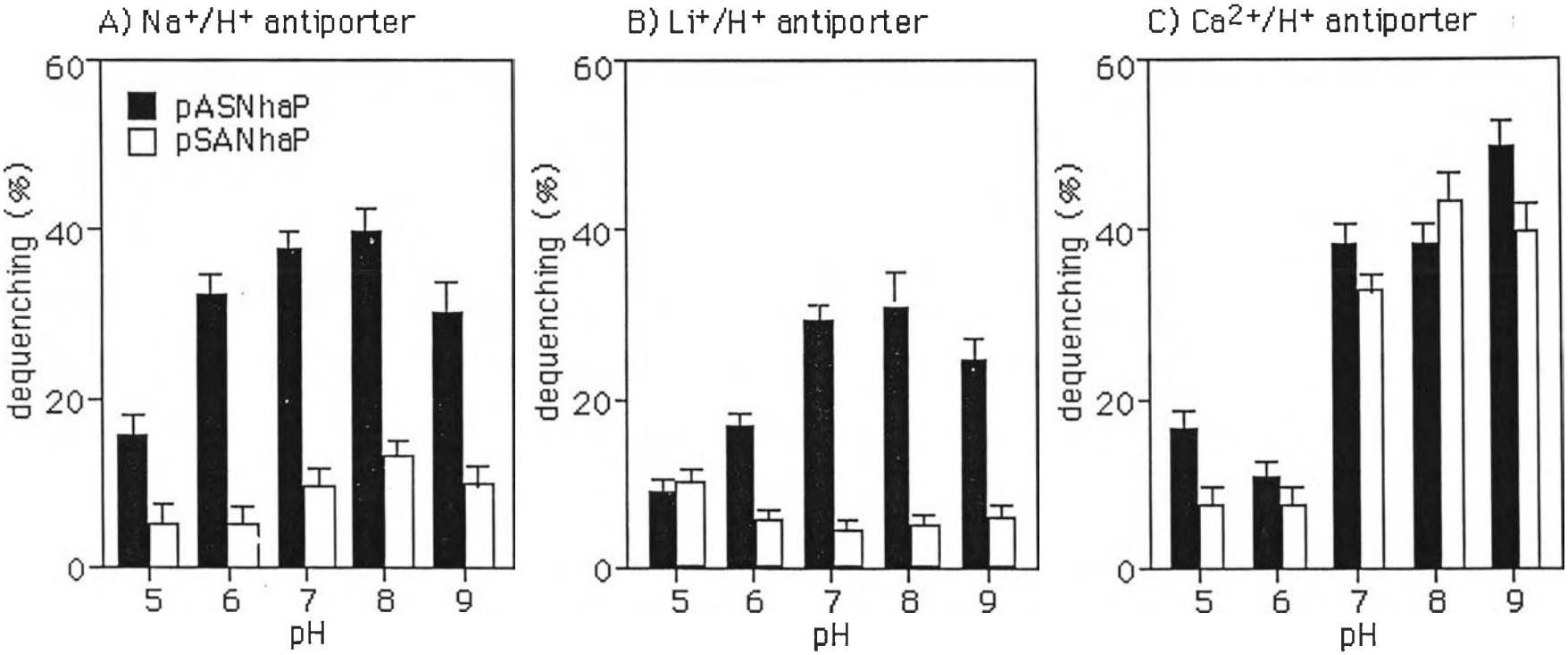

Figure 3.14 The activities of chimeric antiporters. The *E. coli* cells expressing ASNhaP and SANhaP chimeras were grown in LBK medium without addition of extra salts. From these cells the everted membrane vesicles were prepared. The antiporter activity was measured as described in Materials and Methods. Each value shows the average of three independent measurements.

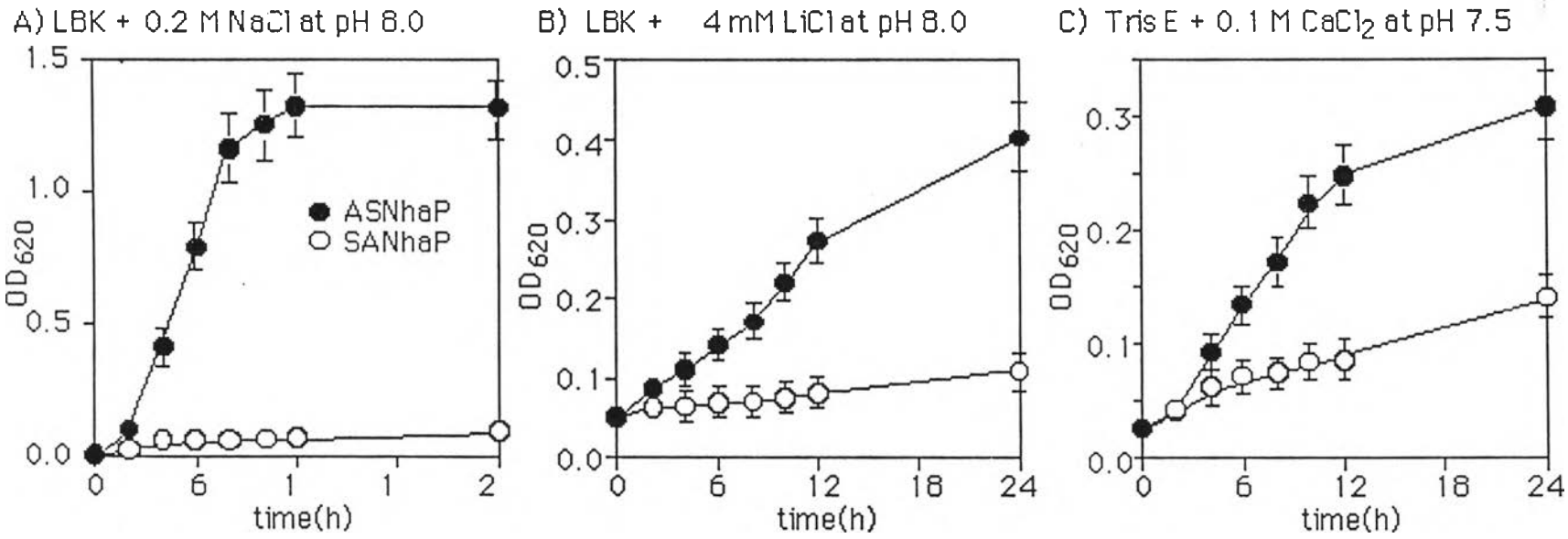

Figure 3.15 Effects of NaCl, LiCl and $CaCl_2$ on the growth rates of *E. coli* cells expressing ASNhaP and SANhaP chimera. The *E. coli* cells expressing ASNhaP and SANhaP chimeras at logarithmic phase in LBK medium were transferred to the LBK medium containing 0.2 M NaCl or 0.4 mM LiCl or TrisE medium containing 0.1 M $CaCl_2$. Other experimental conditions were the same as those in Fig. 3.6. Each value shows the average of three independent measurements.

3. 1. 5 Quantitation of ApNhaP mRNA expression level in intact *A. halophytica* upon the salinity change by Real-time Quantitative RT-PCR

Total RNAs from *A. halophytica* upon the upshock and downshock condition were extracted and analyzed with 1.2 % agarose gel electrophoresis as shown in Figure 3.16. Quantitation of ApNhaP mRNA expression level was carried out using a TaqMan fluorescent chemical analysis method. TaqMan probe and clone specific primers (Taq-F and Taq-R) were optimized for giving the maximum ΔRn. The optimized concentrations for Taq-F, Taq-R and Taq probe was 50, 900 and 900 nM, respectively. Upon the upshock of salinity, ApNhaP mRNA expression level was increased about 4-fold after 30 min upshock and start to decrease after 60 min (Figure 3.17A). Similar pattern was also obtained by downshock. In this case, the level of mRNA was increased about 1.5-fold after 30 min downshock and decreased to the same level after 60 min (Figure 3.17B).

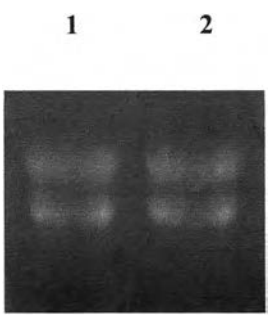

Figure 3.16 Analysis of total RNAs isolated from salt shocked *A. halophytica* on 1.2 % agarose gel electrophoresis

Lane 1 : Total RNAs (3 μg) from salt downshock

Lane 2 : Total RNAs (3 μg) from salt upshock

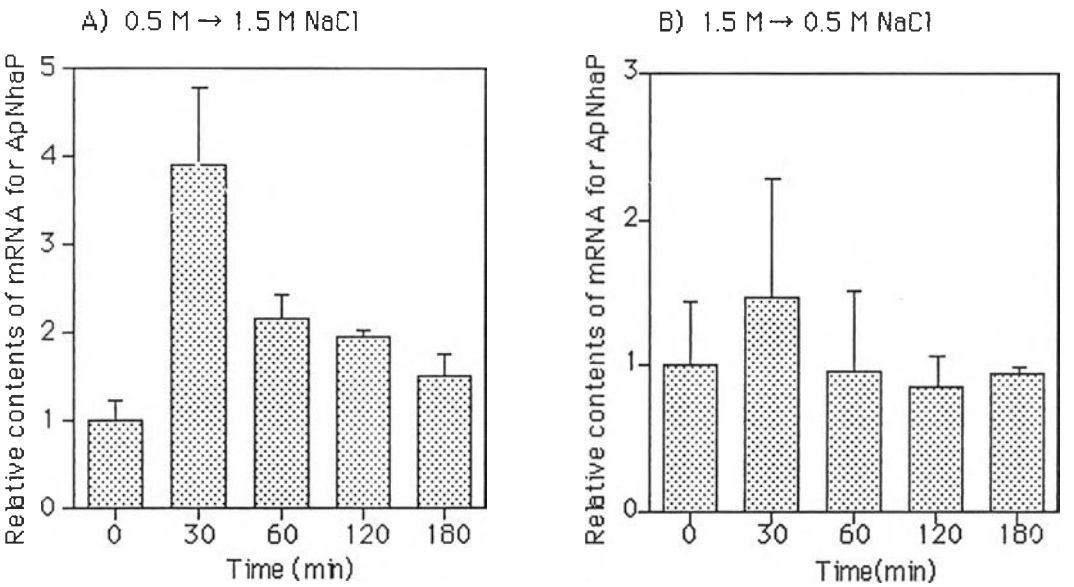

Figure 3.17 ApNhaP mRNA expression level in intact *A. halophytica* after salt shock

A) after upshock B) after downshock

3. 1. 6 Immunoblotting of membrane protein of pANhaP expressing cells

Everted membrane vesicles of pANhaP expressing cells and control cells were used for immunoblotting. Fig 3.18 reveals that the *E. coli* cells transformed with pANhaP exhibited a single cross-reaction band corresponding to approximately 53 kDa whereas the *E. coli* cells transformed with the vector alone (pTrcHis2C) did not show any band. These results indicate that the ApNhaP could be expressed and assembled in *E. coli* membranes.

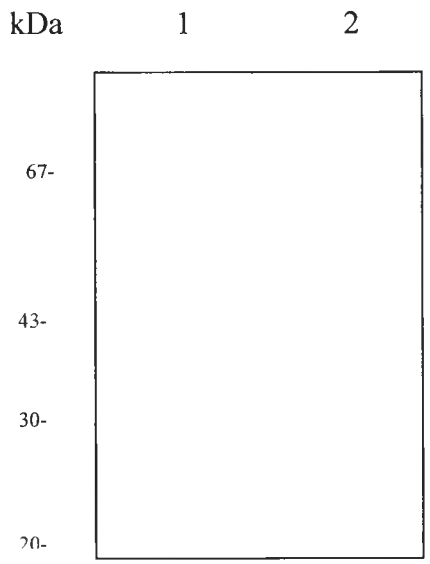

Figure 3.18 Immunoblot analyses of pANhaP expressing cells

Lane 1 : pANhaP expressing cells (50 μg membrane protein)

Lane 2 : control (vector alone pTrcHis2C) cells (50 μg membrane protein)

3. 2 Degradation of glycinebetaine in *A. halophytica*

3. 2. 1 Conditions for the induction of betaine-homocysteine methyltransferase in *A. halophytica*

The growth conditions which might affect the level of intracellular glycinebetaine was examined. Figure 3.19 shows the disappearance of glycinebetaine in *A. halophytica* when cells were subjected to salt downshock from 2.0 M to 0.5 M NaCl. Additional decrease of glycinebetaine was observed when salt downshock treatment was combined with dark treatment. In the control where cells were kept at 2.0 M NaCl condition, the level of intracellular was hardly changed. To search for the enzyme responsible for the reduction of intracellular glycinebetaine. The activity of BHMT of cells was examined when cells were subjected to salt downshock from 2.0 M to 0.5 M NaCl. Enzyme activity increased sharply for the first 3 h of salt downshock. The activity then declined progressively for the next 33 h of salt downshock. Glycinebetaine content fell sharply for the first 3 h and continued to fall as a slower rate (Fig. 3.20).

When cells are deprived of carbon and nitrogen which are essential elements for growth and survival, it is interesting to examine whether this phenomenon affects the activity of BHMT in *A. halophytica*. Figure 3.21 shows the effect of carbon and nitrogen starvation on BHMT activity and glycinebetaine level. The glycinebetaine only slightly decreased after the cells were deprived of carbon and nitrogen for 12 h. Higher rate of decrease of GB occurred for the next 12 h after which the level of glycinebetaine was hardly changed. The activity of BHMT was not affected during the first 12 h of carbon and nitrogen stavation. However, an increase in enzyme activity was observed after 12 h. The increase of BHMT activity was accompanied by the decrease of glycinebetaine level suggesting the role of BHMT to provide energy requirement of the cells by degrading glycinebetaine.

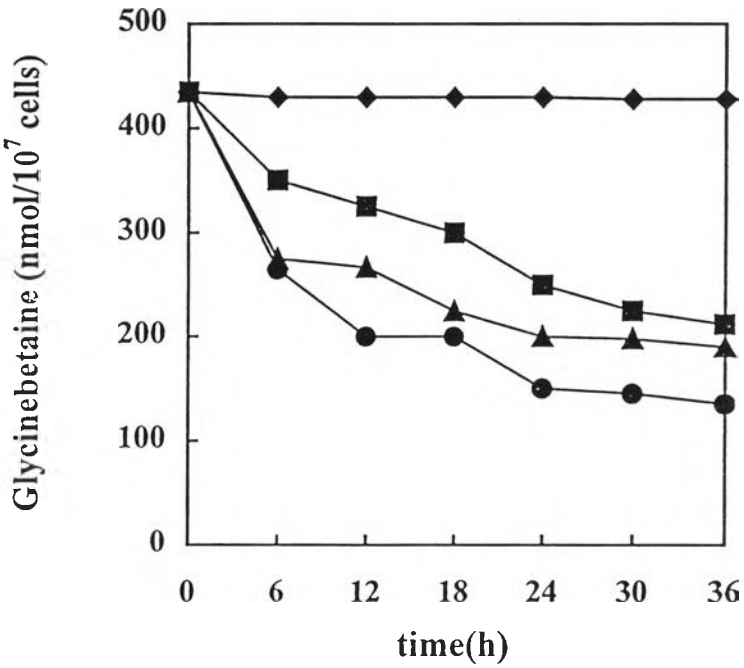

Figure 3.19 Effect of salt downshock on glycinebetaine level. Salt downshock was done by transferring cells from 2.0 M NaCl medium to 0.5 M NaCl for the time indicated, square ; Salt downshock treatment was combined dark condition, triangle ; and also with dark condition and the omission of carbon and nitrogen sources, circle ; The control was the maintenance of cells in 2.0 M NaCl medium, diamond.

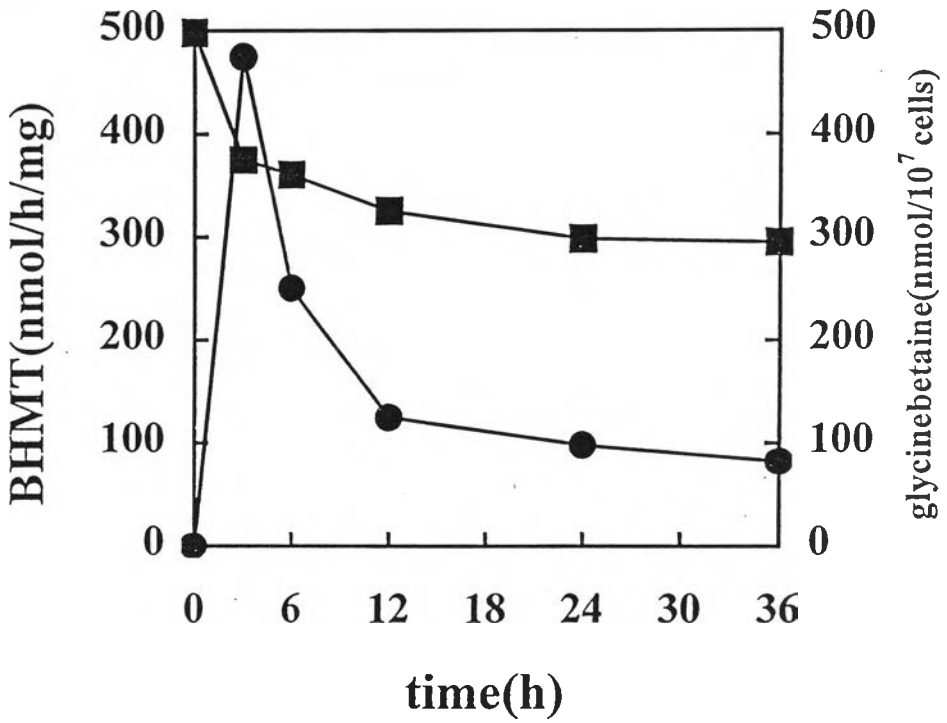

Figure 3.20 Activity of BHMT and level of glycinebetaine in response to saltshock. Cells initially grown in 2.0 M NaCl medium were transferred to 0.5 M NaCl. Cells were extracted at the indicated times for BHMT activity. BHMT activity, closed circle ; Glycinebetaine level, closed square

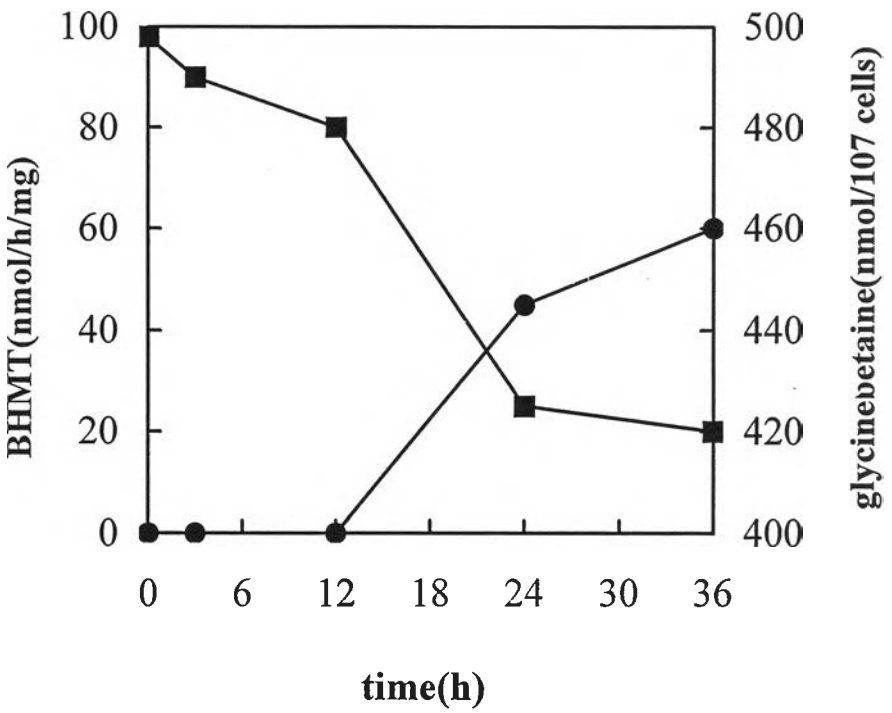

Figure 3.21 Effect of carbon and nitrogen starvation on BHMT activity and glycine betaine level. Cells were grown in 2.0 M NaCl medium for 7 days, after which the cells were transferred to a fresh 2.0 M NaCl medium lacking carbon and nitrogen source. At the time indicated, cells were extracted for BHMT activity and glycinebetaine.

BHMT activity, closed circle ; Glycinebetaine level, closed square

3. 2. 2 Determination of intermediate products(s) of BHMT activity

According to the protocol described in step 2. 8. 2, the presence of *N, N*-dimethylglycine was determined. After labelling *A. halophytica* with ^{14}C-glycinebetaine under salt downshock condition, the radioactive compound (s) in cells was identified by TLC and visualized by autoradiograph.

Figure 3.22 showed the autoradiogram of *N, N*-dimethylglycine present in the extract of *A. halophytica* cells after salt downshock 24 h and 48 h, respectively.

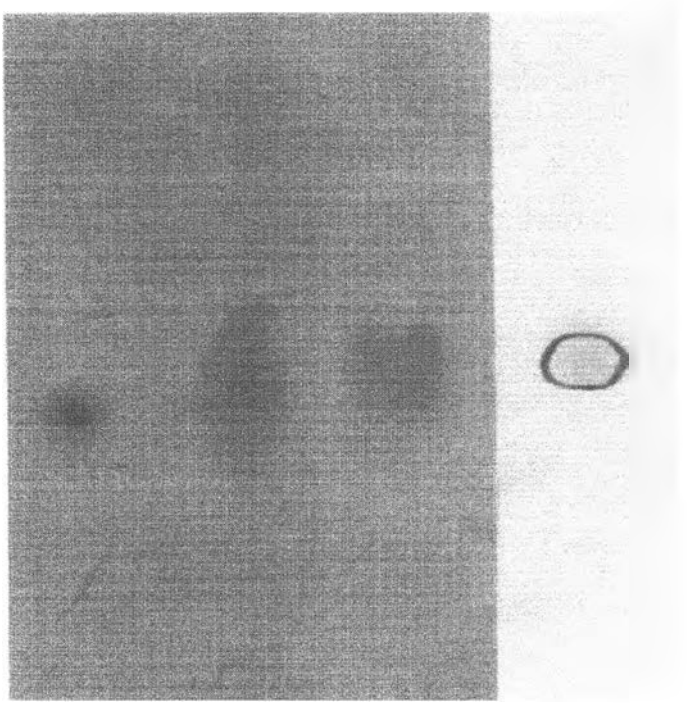

Figure 3.22 Autoradiogram of radioactive compound(s) extracted from intact cell of *A. halophytica* under hypoosmotic stress.

Lane 1 : ^{14}C-glycinebetaine

Lane 2 : ^{14}C-intermediate product(s) after salt downshock for 24 h

Lane 3 : ^{14}C-intermediate product(s) after salt downshock for 48 h

Lane 4 : *N, N*-dimethylglycine standard

3. 3. 3 Purification of BHMT and its properties

BHMT from *A. halophytica* was purified by hydroxyapatite, Sepharose CL-6B and Sephadex G-200 column chromatography, respectively. For hydroxyapatite column (Fig.3.23), the BHMT protein was approximately purified 4-fold. The next step, Sephadex CL-6B (Fig.3.24), effectively removed the bulk of undesired proteins. Slight improvement of the purity of the enzyme was obtained after Sephadex G-200 column (Fig.3.25). A typical purification of BHMT from *A. halophytica* is summarized in Table 2. The enzyme was purified 24-fold after 3 steps of column chromatography, giving a purified enzyme with a specific activity of 595 nmol $h^{-1}mg^{-1}$. The molecular weight of native BHMT was estimated to be 350 kDa from Sephadex G-200 chromatography (Fig. 3.26). And analysis by SDS-PAGE showed a single band of 45 kDa (Fig. 3.27). These results suggest that *A. halophytica* BHMT is likely an octamer of 45 kDa subunits.

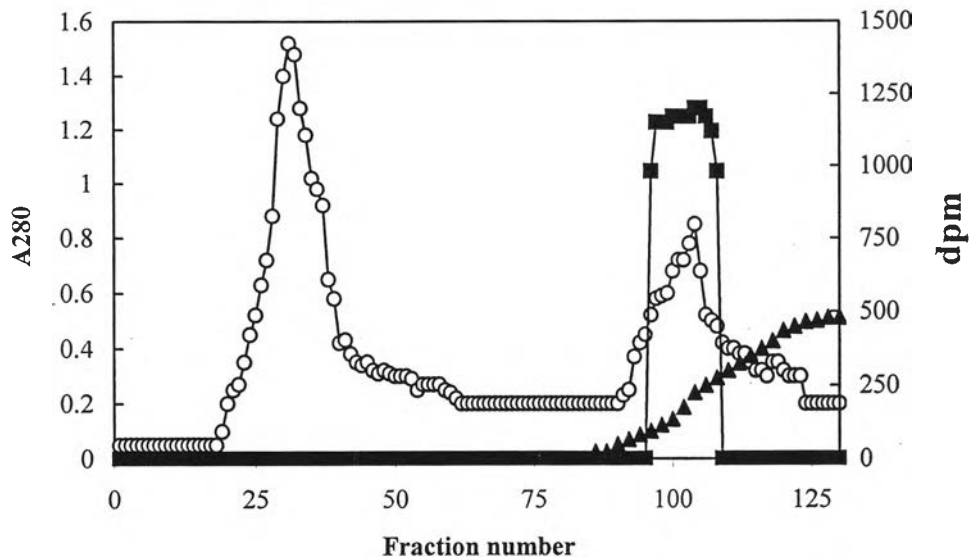

Figure 3.23 Hydroxyapatite chromatography of *A. halophytica* BHMT.

A280, open circle ; BHMT, closed square ;

Potassium phosphate buffer concentration (mM), closed triangle

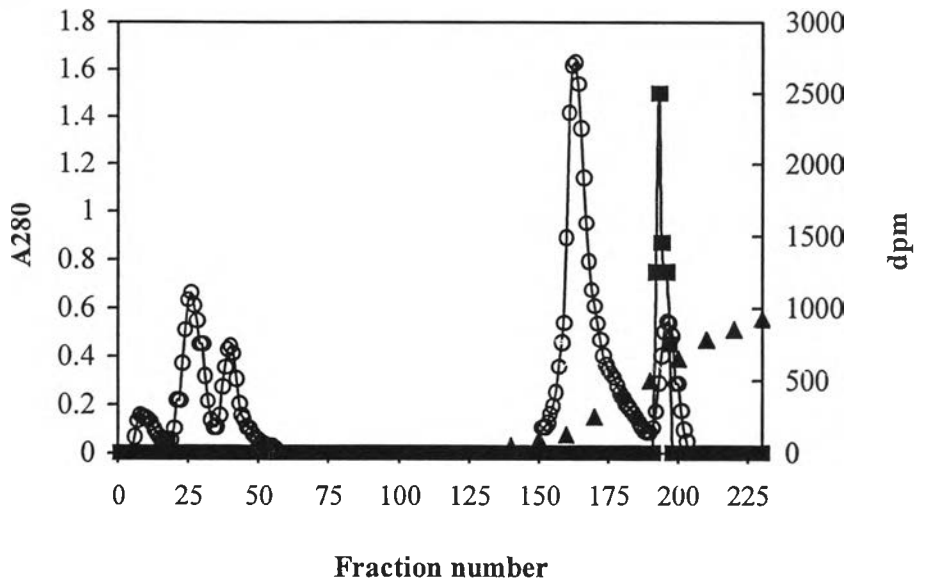

Figure 3.24 Sepharose CL-6B chromatography of *A. halophytica* BHMT.

A280, open circle ; BHMT, closed square ;

KCl concentration(mM), closed triangle

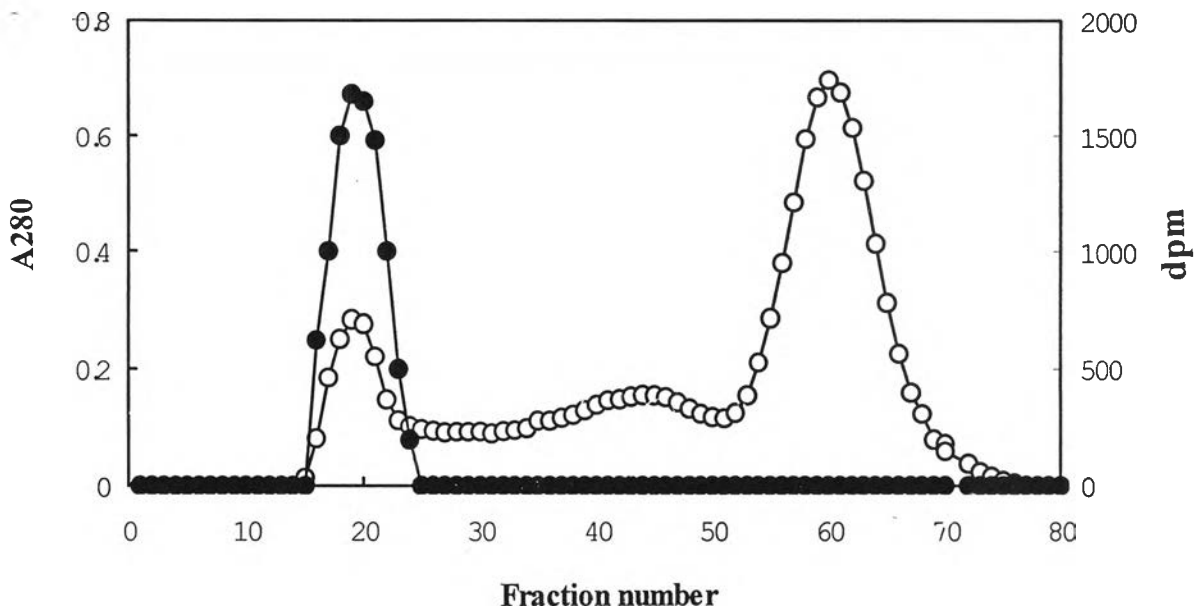

Figure 3.25 Sephadex G-200 chromatography of *A. halophytica* BHMT.

A280, open circle ; BHMT, closed circle

Purification step	Protein (mg)	Activity (nmol/h)	Specific activity (nmol/h/mg)	Purification (fold)	Yield (%)
1. Crude	232.5	5727	25	1	100
2. Hydroxyapatite	28.8	2642	92	4	46
3. Sepharose CL-6B	4.2	2093	498	20	37
4. Sephadex G-200	1.1	655	595	24	11

Table 2 Purification of BHMT from *A. halophytica*

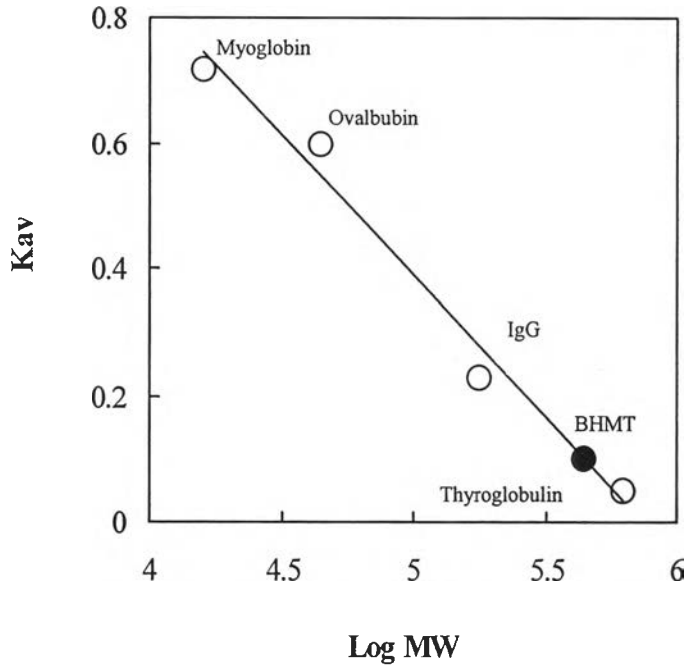

Figure 3.26 Estimation of molecular mass of *A. halophytica* BHMT by gel fitration chromatography

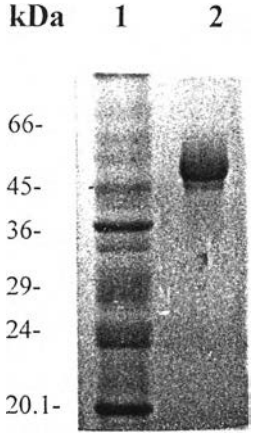

Figure 3.27 Estimation of molecular mass of *A. halophytica* BHMT by SDS-PAGE

Lane 1 : Standard protein marker

Lane 2 : Purified BHMT

The partial purified of BHMT was studied for its properties. Figure 3.28 shows the pH profile with an optimum at pH 7.5 with a slight decrease in activity at either pH 7.0 or 8.0. The optimum temperature for BHMT activity occurred at 37°C (Fig. 3.29) At higher temperature of 45°C, the enzyme still remained some activity with about one-fourth of that abserved at 37°C. Apperent Km values as determined by Lineweaver-Burk plot for substrates glycinebetaine and L-homocysteine were found to be 4.3 mM and 1.3 mM, respectively (Figures 3.30 and 3.31). Vmax value of BHMT when glycinebetaine was a variable substrate was 645 nmol h^{-1} mg^{-1}.

The inhibition by substrate analog and salt(NaCl) was tested for inhibitory effect on BHMT activity. Table 3 shows the inhibitory effect of four compounds bearing resemblance to glycinebetaine substrate on BHMT activity. Betaine aldehyde was the most potent inhibitor resulting in the complete loss of enzyme activity. Choline inhibited 60% of the enzyme activity. Slight inhibitory effect was observed for sarcosine. Marked inhibition occurred with dimethylglycine yielding about one-third of the original activity. The presence of NaCl also inhibited the activity of BHMT (Table 4). Half of the original activity was retained at 100 mM NaCl. The concentration of NaCl at 200 mM or higher resulted in a total loss of enzyme activity.

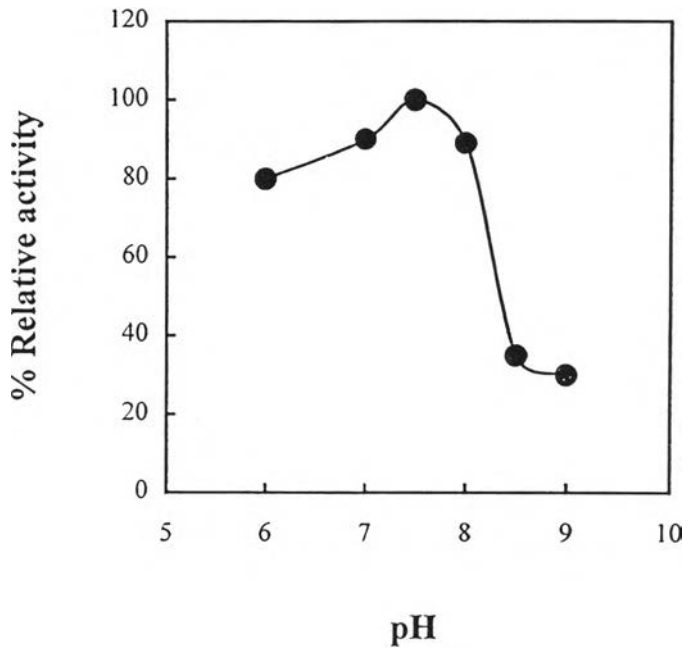

Figure 3.28 Effect of pH on BHMT activity

(1) 50 mM Potassium phosphate buffer pH 6.0

(2) 50 mM Potassium phosphate buffer pH 7.0

(3) 50 mM Potassium phosphate buffer pH 7.5

(4) 50 mM Hepes-KOH buffer pH 8.0

(5) 50 mM Tris-Cl buffer pH 8.5

(6) 50 mM Tris-Cl buffer pH 9.0

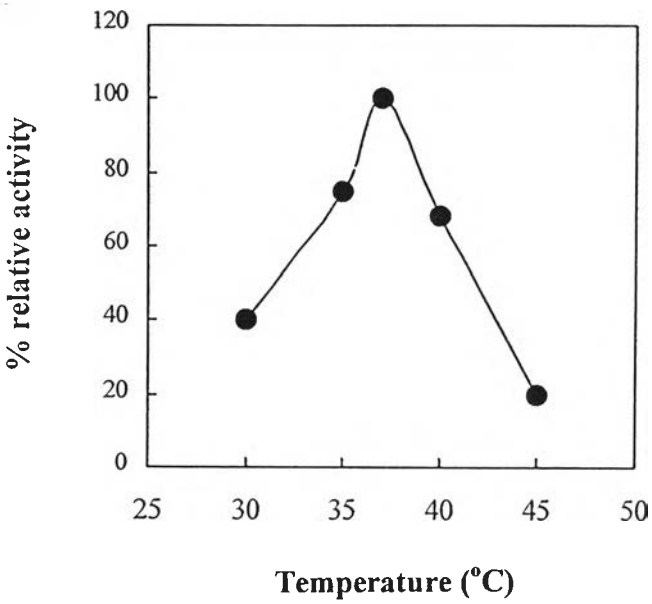

Figure 3.29 Effect of temperature on BHMT activity

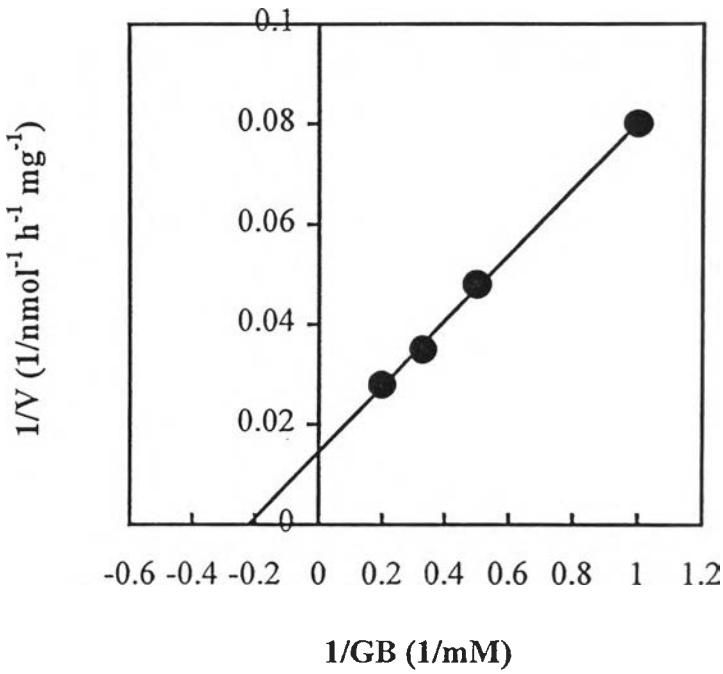

Figure 3.30 Double reciprocal plot of activity of partially purified BHMT as a function of the concentration of the substrate, glycinebetaine

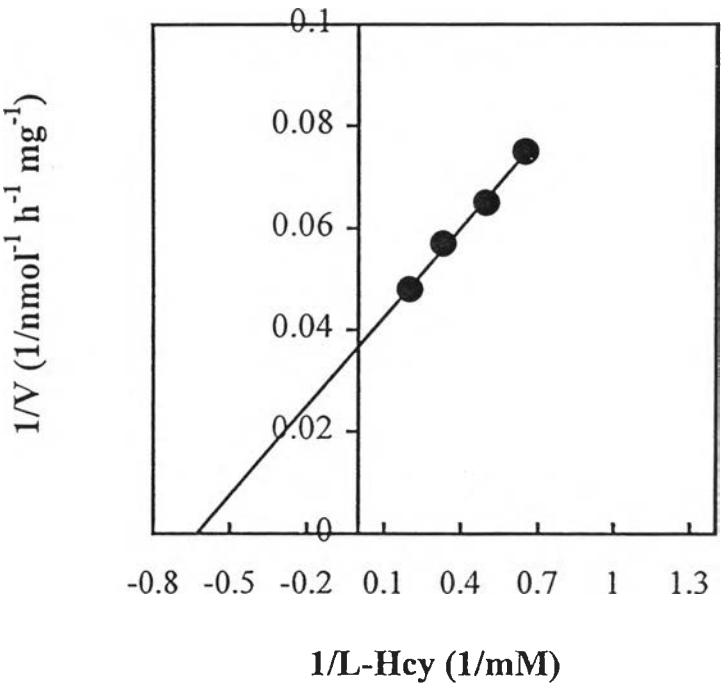

Figure 3.31 Double reciprocal plot of activity of partially purified BHMT as a function of the concentration of the substrate, L-homocysteine

Table 3 Effect of substrate analog on BHMT activity

Compound added	**Relative activity**
None	100
2 mM dimethylglycine	36
5 mM dimethylglycine	30
2 mM Sarcosine	96
5 mM Sarcosine	90
5 mM Choline	40
2.5 mM Betaine aldehyde	0

Table 4 Effect of NaCl on BHMT activity

mM NaCl	Relative activity
0	100
100	50
200	0
300	0
500	0
1000	0